2005

Terdiurnal Wave Signatures in the Upper MesosphericTemperature and Their Association With the Wind Fields at Low-latitudes (20°N)

A. Taori

Michael J. Taylor
Utah State University

S. Franke

Recommended Citation
Taori, A., M.J. Taylor and S. Franke, Terdiurnal wave signatures in the upper mesospheric temperature and their association with the wind fields at low-latitudes (20°N), J. Geophys. Res. Atmos., 110, D09S06, doi:10.1029/2004JD004564, 2005.

Terdiurnal wave signatures in the upper mesospheric temperature and their association with the wind fields at low latitudes (20°N)

A. Taori and M. J. Taylor
Center for Atmospheric and Space Sciences, Utah State University, Logan, Utah, USA

S. Franke
Department of Electrical and Computer Engineering, University of Illinois, Urbana, Illinois, USA

Received 22 January 2004; revised 6 October 2004; accepted 13 December 2004; published 26 March 2005.

[1] A novel investigation of terdiurnal (8-hour) oscillations in the mesosphere and lower-thermosphere temperature and wind field over Maui, Hawaii (20.8°N, 156.2°W) has been performed. Coincident observations using a mesospheric temperature mapper and a meteor wind radar were obtained since May 2002 as part of the Maui Mesosphere and Lower Thermosphere (Maui MALT) program to investigate the seasonal structure and dynamics of the low-latitude middle atmosphere. This study focuses on a 10-day period in July 2002 when a persistent ~8-hour oscillation was identified in dual measurements of the OH (6,2) and O_2 (0,1) nocturnal rotational temperatures sampled at nominal altitudes of 87 and 94 km, respectively. During the summer months, the semidiurnal and diurnal tidal temperature components are expected to be minimal, and these data are most suitable for investigating the terdiurnal wave component, which is usually much weaker. Our results show that the primary 8-hour oscillation observed during this 10-day period exhibited a mean amplitude ~5.5 K and a well-defined phase shift (~1-hour) between the OH and O_2 temperatures (with the O_2 oscillation always leading). The downward phase progression and inferred mean vertical wavelength of ~63 km are most consistent with that expected for the terdiurnal tide. Coincident meteor radar measurements also show an intermittent 8-hour periodicity in the wind data. In particular, a detailed comparison of the winds and temperatures over a 4-day interval within this period suggests a significant correlation indicating a near in-phase temperature relation with the meridional wind component and a near-antiphase relation with the zonal wind component. Comparison of the OH and O_2 8-hour temperature amplitudes also shows strong evidence for highly variable wave dissipation, with amplitude growth factors ranging from 0.6 to 1.9 throughout this period.

Citation: Taori, A., M. J. Taylor, and S. Franke (2005), Terdiurnal wave signatures in the upper mesospheric temperature and their association with the wind fields at low latitudes (20°N), *J. Geophys. Res.*, *110*, D09S06, doi:10.1029/2004JD004564.

1. Introduction

[2] Thermal tides and planetary waves are known to dominate the energetic and dynamics of the mesosphere and lower thermosphere (MLT) region (~80–100 km) due to their large amplitudes in the horizontal and vertical wind fields. Thermal tides are vertically propagating waves excited by differential absorption of solar energy in the troposphere and stratosphere, predominantly by water vapor and ozone. They are global in scale, owing to the nature of their forcing, and exhibit periodicities equal to the solar day or its subharmonics. The most important tides are the diurnal (24-hour) and semidiurnal (12-hour) migrating components which exhibit a westward phase velocity (i.e., they migrate with the apparent motion of the Sun). To date, most studies have focused on the diurnal and semidiurnal tidal components; however, in recent years, observational and modeling evidence supporting a strong, but intermittent terdiurnal tidal signature at MLT heights has been accumulating [*Hocking and Thayaparan*, 1997; *Pendleton et al.*, 2000; *States and Gardner*, 2000; *Smith*, 2000]. There are two competing mechanisms for the terdiurnal tidal component: direct thermal excitation or a nonlinear interaction between the semidiurnal and diurnal tidal modes with considerable seasonal and latitudinal variability [*Smith and Ortland*, 2001].

[3] Measurements of tides in the MLT region have primarily been made from satellites [e.g., *Hays et al.*, 1994; *Burrage et al.*, 1995; *Shepherd et al.*, 1995], and from ground-based MF and meteor radars [e.g., *Manson et al.*, 1989; *Franke and Thorsen*, 1993; *Hocking and Thayaparan*, 1997; *Hocking and Hocking*, 2002], and Rayleigh and resonant lidars [e.g., *Dao et al.*, 1995; *States and Gardner*, 2000; *She et al.*, 2003]. Together these studies have provided a wealth of data on the temporal and latitudinal structure of

0148-0227/05/2004JD004564

the 12- and 24-hour solar tides. Remote sensing measurements of the naturally occurring airglow emissions also provide an important tool for investigating tidal influences on the upper atmospheric dynamics. Pioneering studies on the influence of tides on the MLT airglow emissions were initially conducted by *Fukuyama* [1976] and *Petitdidier and Teitelbaum* [1977]. Subsequently, there had been several reports in the literature using ground-based observations of the 12- and 24-hour tidal signatures in the airglow emissions [e.g., *Takahashi et al.*, 1984; *Walterscheid et al.*, 1986; *Hecht et al.*, 1998; *Sivjee and Hamwey*, 1987]. However, the finite length of the nocturnal airglow data sets often limits their tidal interpretation. Nevertheless, useful information on the tides can be extracted from such data sets [*Crary and Forbes*, 1983].

[4] Terdiurnal oscillations in the MLT wind field were first detected using meteor radar measurements [*Revah*, 1969]. Subsequently, several observational and modeling investigations have revealed the existence of terdiurnal wind oscillations of limited duration but significant amplitude (typically up to ~20 m/s) in the MLT region [*Glass and Fellous*, 1975; *Teitelbaum et al.*, 1989; *Thayaparan*, 1997; *Akmaev*, 2001; *Younger et al.*, 2002; *Namboothiri et al.*, 2004]. In contrast, there have been very few reports of the presence of 8-hour oscillations in the airglow emissions. Initial measurements of 8-hour signatures in airglow emission intensity were conducted from high latitudes to take advantage of the long polar nights [*Sivjee et al.*, 1994; *Oznovich et al.*, 1995]. However, more recent measurements from midlatitudes show strong evidence of terdiurnal oscillations in mesospheric temperature [*Wines et al.*, 1995; *Taylor et al.*, 1999; *Pendleton et al.*, 2000]. Together these measurements provide independent evidence in support of the MLT wind measurements of the terdiurnal tidal signature at high and midlatitudes.

[5] As part of the Maui Mesosphere and Lower Thermosphere (Maui MALT) program, the Utah State University Mesospheric Temperature Mapper (MTM) has been operated at Maui, Hawaii (HI) (20.8°N, 156.2°W) since November 2001 to investigate variability in mesospheric temperatures at low latitudes. As expected, the data were dominated by long-period tidal signatures throughout the year [e.g., *Dao et al.*, 1995; *Hecht et al.*, 1998]. However, our data for July 2002 suggest that MLT temperatures measured at two altitudes were characterized by a persistent ~8-hour oscillation. This paper focuses on measurements obtained during 5–18 July 2002, when the global scale wave model (GSWM) [*Hagan et al.*, 1995] indicates a minimum in amplitude for the diurnal and semidiurnal tidal components in temperatures at this latitude. The MTM data have been used to investigate the properties of this oscillation (periodicity, amplitude, phase propagation and growth), which appears to be tidal in nature. These results were then compared with coincident meteor radar measurements of the MLT wind field to perform a unique investigation on the mesospheric wind and temperature relationship for this tidal component.

2. Instrumentation and Observations

[6] The Maui MALT program is a joint research initiative between the U.S. Air Force Office of Scientific Research (AFOSR) and the National Science Foundation (NSF) designed to investigate the dynamics of the low-latitude middle atmosphere in unprecedented details. As part of this program a cluster of optical instruments has been operated from the Air Force AEOS facility at the summit of Haleakala Crater, Maui, since November 2001. These instruments include a powerful Na wind-temperature lidar (operated on a campaign basis) and several passive imaging instruments designed for long-term unattended measurements of the MLT airglow emissions. Since May 2002, the optical measurements have been complemented by continuous meteor radar observations of the ~80–100 km wind field over Maui, HI. This paper focuses on joint measurements collected by the Utah State University Mesospheric Temperature Mapper (MTM) and the University of Illinois Meteor Wind Radar (MWR).

2.1. Mesospheric Temperature Mapper

[7] The Mesospheric Temperature Mapper (MTM) was developed in 1997 under the NSF Coupling Energetics and Dynamics of Atmospheric Regions (CEDAR) program to enhance upper atmospheric imaging capabilities. The MTM is a high performance, solid state imaging system capable of determining wave-induced fluctuations in the intensity and rotational temperature of the OH (6,2) Meinel band, and was recently enhanced to include the O_2(0,1) atmospheric band emission. The MTM utilizes a large format (6.45 cm^2), 1024 × 1024 pixel CCD array coupled to a 90° circular field of view telecentric lens system. The high quantum efficiency (~50% at near infrared wavelengths) and low noise characteristics (dark current ~0.1 e^-/pixel/s at −50°C) of the CCD array provide an exceptional capability for high-quality nocturnal measurements of OH and O_2 emission intensities (<0.5% in 1 min) and derived rotational temperatures (precision <1–2 K in 3 min). The inherent linearity and stability of the MTM has also enabled seasonal investigations of the mesospheric temperature variability [*Pendleton et al.*, 2000; *Taylor et al.*, 2001].

[8] In operation, sequential exposures were made using a temperature-stabilized filter wheel fitted with narrow band ($\Delta\lambda \sim 1.2$ nm) filters centered at 840 and 846.5 nm for the OH (6,2) Meinel band and 866 and 868 nm for the O_2 (0,1) atmospheric band measurements, followed by a background sky measurement at 857 nm. To enhance the precision of the temperature determinations the signal-to-noise ratio (SNR) of the data was increased by 8 × 8 binning on the chip to form a 128 × 128 superpixel image with a resultant zenithal foot print of about 0.9 × 0.9 km per superpixel. Rotational temperatures were then computed separately for both emissions using the ratio method, as described eloquently by *Meriwether* [1984].

[9] For example, for the OH (6,2) data the ratio of $P_1(2)$ (840 nm) and $P_1(4)$ (846.5 nm) rotational line emissions, which are known to be in local thermodynamic equilibrium, is used to determine the atmospheric temperatures averaged over the ~8 km thick emission layer centered at ~87 km, using the transition probabilities of *Goldman et al.* [1998] [*Pendleton et al.*, 2000]. A similar procedure was applied to the O_2 data to determine the height-averaged temperature at the ~94 km level.

[10] The MTM derived OH temperatures were validated initially by comparison with simultaneous zenith temperature measurements obtained by the Colorado State University Na

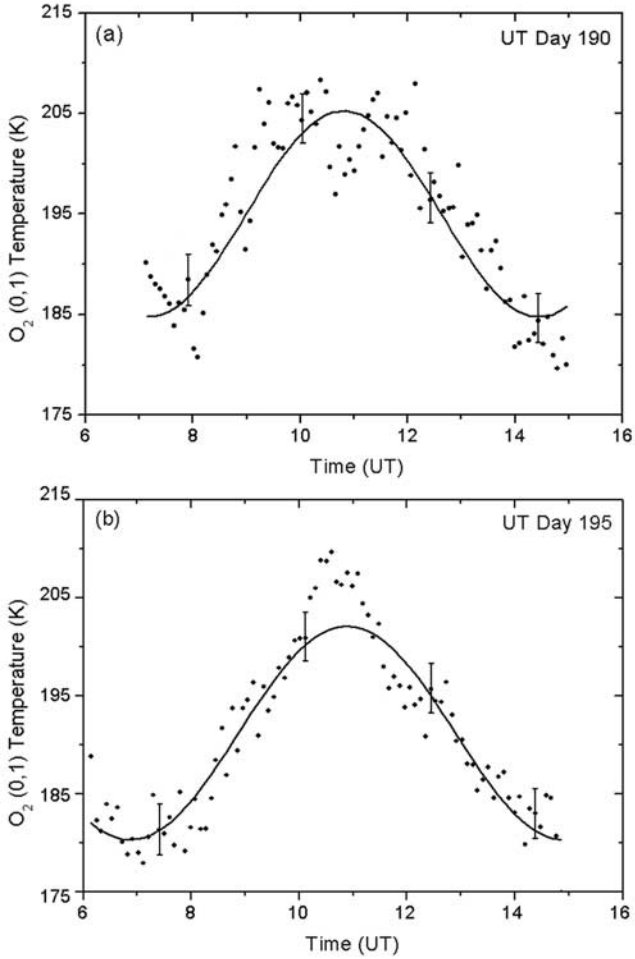

Figure 1. Time series showing raw (~3 min) MTM O_2 (0–1) temperature data (a) for 8–9 July 2002 (UT day 190) and (b) for 13–14 July 2002 (UT day 195). The solid curve in each plot shows an 8-hour fit to the data (which also exhibits some smaller-scale gravity wave variability). Example error bars illustrate the precision in the individual temperature estimates.

temperature lidar [*Pendleton et al.*, 2000]. Most recently, both the OH and O_2 temperature data have been compared with temperature soundings by the University of Illinois wind-temperature lidar as part of the Maui MALT program. The mean nocturnal temperatures and their temporal variability, as measured by these two different instrumental techniques, were found to be in very good agreement with mean nightly differences of less than ±5 K for assumed emission altitudes of 87 km (OH) and 94 km (O_2). A detailed comparison of the OH and O_2 temperatures with coincident lidar measurements is given by *Zhao et al.* [2005].

[11] Figures 1a and 1b show two examples of the raw O_2 temperatures derived from the MTM data recorded on 8–9 and 13–14 July 2002 (UT days 190 and 195) respectively. For comparison, both data sets are plotted on the same scales. For each emission layer a temperature determination is made every ~5 min (note: the example "error bars" show the uncertainty in the individual temperature determinations). The high quality of the data throughout the ~9-hour observing interval is evident and each plot shows a well-defined long-period oscillation (of primary interest here) with superimposed smaller-scale gravity waves of periodicities ~1–2 hours. This is emphasized by the solid curve in both plots which show a fixed 8-hour period least squares fit to the raw data sets revealing a peak-to-trough variation of ~20 K in each case. During the interval 5–18 July 2002 (UT days 187–200), well-defined wave structures exhibiting coherent ~8-hour periodicities were observed in the OH and O_2 temperatures and their associated emission intensities (not shown) on almost every night.

2.2. Meteor Wind Radar

[12] The Maui MALT meteor radar is located at Kihei, Maui (20.8°N, 156.4°W) and operates at 40.92 MHz. Meteor trail reflections are coherently detected on each of five 3-element Yagi antennas oriented along two orthogonal baselines, with one antenna located in the center of the array common to both baselines. On each baseline the outer antennas are separated from the central antenna by 1.5 and 2.0 wavelengths, respectively. This configuration helps to minimize antenna coupling, provides enough redundancy to unambiguously determine the azimuth and elevation of most meteor echoes, and enables excellent angular resolution for position determination. The average transmitted power is approximately 170 W, which results from a 13.3 microsecond pulse length, 6 kW peak envelope power, and an interpulse period (IPP) of 466 microseconds. The relatively high PRF causes meteor echoes to be range aliased; however, the relatively narrow height distribution of meteor echoes combined with precise azimuth and elevation angle determination allows any range ambiguities to be resolved. The algorithms used to determine the meteor trail position and Doppler shift are described in detail in the work of *Hocking and Thayaparan* [1997]. Wind velocities are estimated from the trail positions and Doppler shifts using a weighted least squares fit to an assumed constant wind vector composed of eastward and northward components. (The vertical wind is assumed to be negligible.) The wind vector fit is based on echoes collected within 1 hour time bins.

[13] Figure 2 shows a spectrogram of the meridional winds derived from the meteor radar for a four month period (June to September 2002), encompassing the July

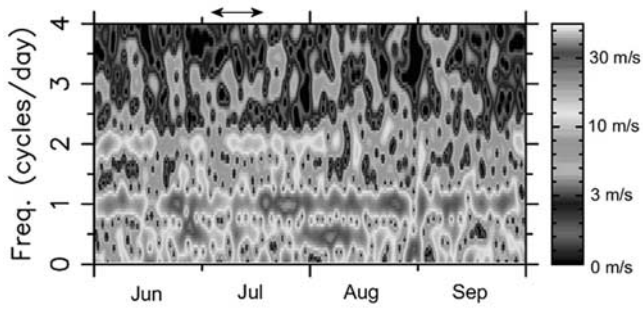

Figure 2. Spectrogram showing the meteor radar meridional winds from June to September 2002, height-weighted and centered on the OH emission layer. Strong diurnal and semidiurnal tidal components are evident together with a weaker and more intermittent terdiurnal tidal signature. The horizontal arrow indicates the observing period where 8-hour waves were detected.

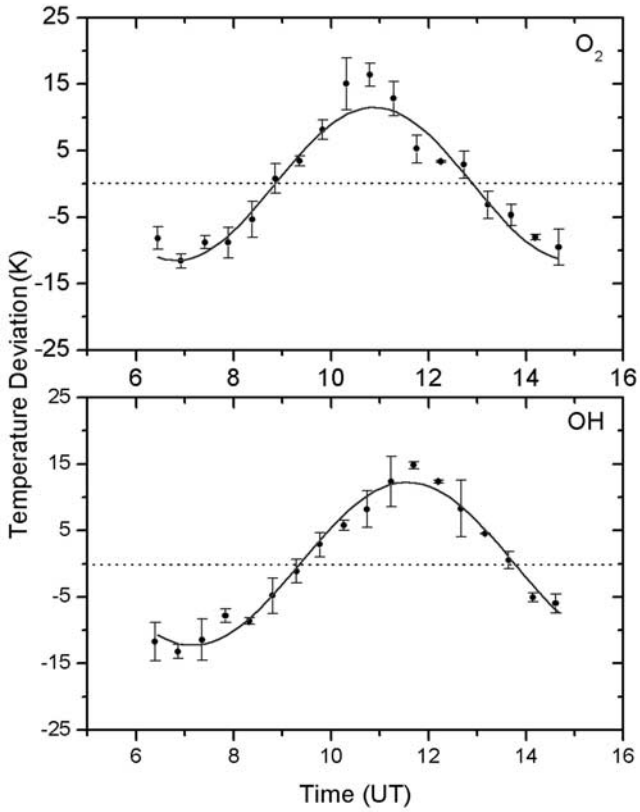

Figure 3. Least squares sinusoidal fit to the O_2 and OH data obtained on UT day 195 (raw O_2 data shown in Figure 1b). In both plots the solid circles show the 0.5-hour averaged temperatures and associated standard deviations in the individual estimates. Best fit results yield a periodicity of 8.8 ± 0.2 hours for the OH data and 7.9 ± 0.2 hours for the O_2 data with the O_2 oscillation leading the OH by ~0.7 hours. Both perturbations have similar amplitudes of ~11–12 K.

period where strong quasi-8-hour wave signatures were detected in mesospheric temperatures by the MTM (indicated by the horizontal arrow on the top of the figure). In this plot the radar wind data have been height-weighted using a function of the form exp $(-(z - z_0)^2/\text{std}^2)$ where, std = 5.5 km, z is the altitude, and z_0 = 85.9 km, approximately centered on the OH emission peak altitude. (A similar analysis was performed for the wind data centered on the O_2 emission layer using z_0 = 91.7 and std = 4.5.) At the OH layer height, wind data show that the tidal perturbations throughout this period were dominated by a diurnal (24-hour) component (wind amplitudes typically >20 m/s) that was somewhat intermittent in nature. The semidiurnal (12-hour) tidal signature was also intermittent in nature and exhibited amplitudes of typically ~10 m/s during June–July with significantly reduced amplitudes during August–September. The terdiurnal tidal wind component was also evident but weaker and more intermittent than the diurnal and semidiurnal components. In particular, the phase of the 8-hour component was found to be highly variable from day-to-day, and when averaged over the key period 5–18 July, the "phase jitter" caused the 8-hour signature to essentially be averaged out. However, when the data were averaged for shorter periods within this window, the phase remained coherent providing a good estimate of the amplitude of the terdiurnal tide. Later, we utilize this result to investigate the wind and temperature relations for long-period quasi-8-hour oscillations observed in the MLT region. At this point it is important to note that in general the wind and temperature tidal harmonics have different amplitude dependencies with latitude; normally, for a given tidal harmonic, the induced horizontal winds are smallest at latitudes where the temperature perturbations are largest and vice versa. This is due to the nature of the Hough functions which describe the global characteristics of wind and temperature tides [e.g., *Chapman and Lindzen*, 1970].

3. Analysis and Results

[14] A total of 12 nights of quality data were obtained during the period 5–18 July 2002. Coherent long-period wave structures were observed on all of these occasions, ten of which exhibited a well-defined ~8-hour periodicity while two indicated significantly longer periodicities close to the semidiurnal tidal harmonic. As the nocturnal date lengths during the summer months at Maui are limited to ~8–9 hours duration this analysis focuses on the dominant ~8-hour periodicity waves.

3.1. Eight-Hour Wave Periodicities and Phase Relationship

[15] Figure 3 illustrates our method of analysis for extracting the principle wave parameters (periodicity, amplitude and phase) characterizing these long-period events observed jointly in the OH and O_2 temperature data. Owing to the nature of the nocturnal measurements, we are not able to remove the diurnal or semidiurnal tidal components from these data in a meaningful manner. In this example, the O_2 data (Figure 1b) and the corresponding OH data recorded on 13–14 July are plotted. To limit the effects of small-scale gravity waves, the MTM data were first averaged into 0.5-hour bins and then subtracted from the mean nocturnal values to yield the mean temperature deviations associated with the primary wave perturbations [e.g., *Pendleton et al.*, 2000]. On this occasion, the mean nocturnal temperature was 190.8 K at the altitude of the O_2 layer and 180.1 K for the OH layer. The individual error bars on each plot indicate ±1 standard deviation of the averaged data which, as mentioned earlier, are dominated by small-scale geophysical variability. The solid curves in both plots indicate a simple least squares fit to the 30-min averaged temperature data set using the following wave equation:

$$Y = A\cos\left[\pi\frac{(X - Xc)}{W}\right],$$

where A is the amplitude of the fitted wave of half-period W with phase Xc, and X is the time. On this night, the O_2 data exhibited a best fit wave period of 7.9 ± 0.2 hours with amplitude of 11.2 ± 0.5 K, and a peak in the temperature wave at 1018 UT. In comparison, the OH emission exhibited a similar wave periodicity of 8.8 ± 0.2 hours and perturbation amplitude of 12.2 ± 0.6 K. However, the crest of the OH temperature wave occurred at ~1130 UT, indicating a phase shift of ~0.7 hours with the O_2

Table 1. Results of Wave-Fit Analysis for the 8-Hour Oscillations Observed in the Mesospheric OH and O_2 Temperatures for the Ten Nights of Data[a]

UT Day 2002	Local Date	Data Duration, hours	Wave Period, hours		Wave Amplitude, K		Growth Factor	Phase Difference, hours	Vertical Phase Velocity, m/s
			OH	O_2	OH	O_2			
187	5–6 July	9	7.2 ± 0.2	7.5 ± 0.4	6.5 ± 1.1	10.5 ± 1.7	1.6 ± 0.29	1	1.9
188	6–7 July	9	7.6 ± 0.4	9.8 ± 0.1	9.0 ± 0.8	8.9 ± 0.9	0.9 ± 0.12	0.6	3.2
189	7–8 July	8.5	8.2 ± 0.3	8.2 ± 0.3	6.6 ± 1.0	12.3 ± 1.5	1.8 ± 0.26	0.5	3.8
190	8–9 July	9	8.6 ± 0.1	8.8 ± 0.3	10.5 ± 0.4	10.9 ± 0.6	1.0 ± 0.07	1.2	1.6
191	9–10 July	9	7.8 ± 0.3	8.8 ± 0.5	5.1 ± 0.5	9.6 ± 0.5	1.9 ± 0.21	0.8	2.6
194	12–13 July	9	7.8 ± 0.1	8.1 ± 0.1	9.8 ± 0.4	11.3 ± 0.5	1.1 ± 0.06	0.9	2.1
195	13–14 July	9	8.8 ± 0.2	7.9 ± 0.2	12.2 ± 0.6	11.2 ± 0.5	0.9 ± 0.06	0.7	2.9
196	14–15 July	9	9.8 ± 0.5	9.2 ± 0.2	10.2 ± 0.4	6.3 ± 0.4	0.6 ± 0.05	1.2	1.5
197	15–16 July	8	7.0 ± 0.1	8.2 ± 0.1	16.8 ± 0.7	16.5 ± 0.5	0.9 ± 0.04	0.7	2.6
198	16–17 July	6	7.6 ± 1.3	9.4 ± 0.2	6.7 ± 0.5	7.2 ± 1.0	1.1 ± 0.16	2	0.9

[a]Note the large night-to-night variability in their amplitudes.

perturbation leading the OH signal. This result is consistent with downward phase progression associated with tides or large-scale, long-period gravity waves. Furthermore, the similarity in amplitudes of the two temperature signals indicates very little growth with altitude on this occasion (see discussion).

[16] Table 1 lists the results of our analysis applied to the 10 nights of data that exhibited periodicities close to 8 hours. With the exception of UT days 192 and 193 the data nights are consecutive. The fitted wave periods range from ~7 to 10 hours for both the OH and O_2 data with a mean of 8.0 hours (OH) and 8.5 hours (O_2). Although fits to an individual night's OH and O_2 measurements show some differences in the deduced periodicities, practical limitations imposed by the geophysical variability in these two data sets suggests that in each case these waves are most probably due to the same ~8-hour-type perturbation. These practical limitations are imposed by the variability in the smaller-scale gravity wave content with altitude and by changes in the chemical processes affecting the emission intensities during dusk and dawn period. In particular, the phase shift between the O_2 and OH temperature data (for wave periodicities differing by <1.2 hours), shows the O_2 waves leading their OH counterparts with phase differences ranging from 0.5 to 1.2 hours, consistent with a downward phase progression. (Note: on UT days 188 and 198 the differences in the fitted O_2 and OH periodicities were close to 2 hours and they have not been included in the phase assessment.)

[17] To better investigate the nature of these long-period waves, Figure 4 plots all 10 nights when ~8-hour waves were observed simultaneously in the OH and O_2 temperature data. In this plot, the nightly data have been averaged into 1-hour bins to emphasize the geophysical variability associated with the long-period oscillations. The coherence in the day-to-day oscillations in both the OH and O_2 data sets is most notable. In particular, there is very little night-to-night variation in the phase of the wave perturbation (especially for the O_2 data), resulting in a consistent phase relation (indicated by the bold solid curves in each plot). Figures 5a and 5b quantify this relationship by plotting the "mean nocturnal" temperature variation for each emission altitude throughout this 10-night period. The individual error bars show the standard deviation for the data ensemble (which, as noted above, are dominated by geophysical variability during this period). The solid lines indicate a least squares fit to the data about mean values of 193.6 K for the O_2 emission and 183.6 K for the lower altitude OH emission. In both cases the amplitudes of the mean temperature perturbation were very similar at ~5–6 K. The periods of the fitted sinusoids: 8.4 ± 0.4 hours (O_2) and 9.2 ± 0.3 hours (OH) agree well within the limits of the measurements and demonstrate the sustained and coherent nature of the observed ~8-hour oscillations. To further emphasize the apparent dominance of ~8-hour wave component, Figure 6 re-plots the O_2 temperature data (of Figure 5a) where we have fitted independently a least

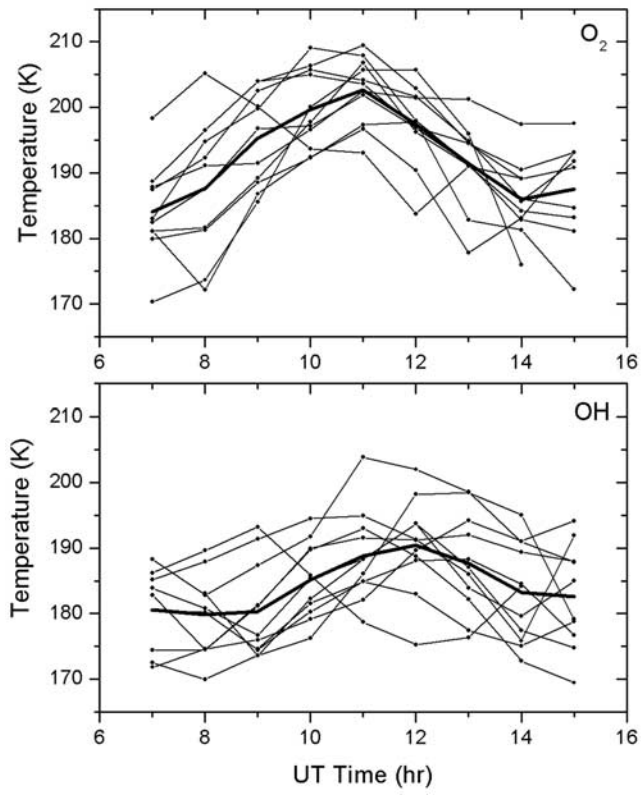

Figure 4. Ensemble of mesospheric OH and O_2 temperature data for the 10 nights of observations. The data have been averaged into 1-hour intervals to emphasize the coherence of the ~8-hour oscillation. The bold line in each plot indicates the mean nocturnal temperature variability during this period.

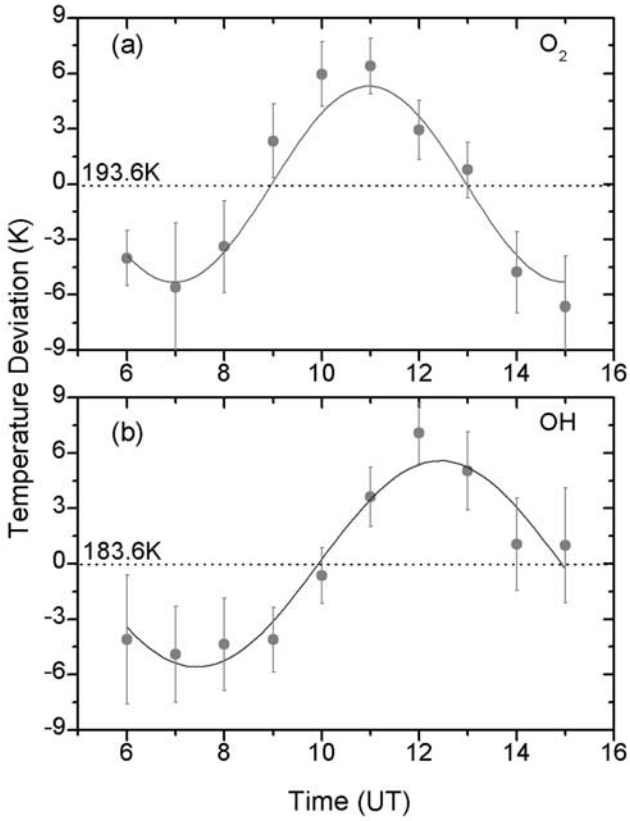

Figure 5. Least squares sinusoidal fit to the average nocturnal mean temperature deviations of Figure 4. Individual error bars depict the uncertainties in the average estimates which were dominated by geophysical variability. A strong terdiurnal signature of amplitude ~5.5 K is evident in both data sets, exhibiting a clear downward phase progression.

squares sine wave of periodicity 6, 8, and 12 hours to illustrate the expected form of these tidal components for comparison with the 10-day data ensemble. The resultant fits yield reduced χ^2 (χ^2/degree of freedom) values of 13.14 (6 hours), 0.99 (8 hours) and 2.82 (12 hours). The high reduced χ^2 values for the 6- and 12-hour fits do not support a quality fit. However, the χ^2 of 0.99 strongly suggests the presence of an 8-hour wave component in the low-latitude upper mesosphere temperature field during July 2002.

3.2. Eight-Hour Wave Amplitudes and Growth

[18] Assuming an OH layer centered at ~87 km and an O_2 layer at ~94 km we can use the fitted wave data to investigate the growth (or decay) in amplitude of the 8-hour waves as they progressed through the upper mesosphere. The results are also listed in Table 1 and show considerable night-to-night variability in the fitted wave amplitudes which varied in magnitude by over a factor of three (from 5 to 17 K) during the 10 nights of near consecutive data. Comparison of the OH and O_2 data sets indicates strong evidence for amplitude growth or attenuation on individual nights. This property of the waves can be quantified by taking the ratio of the O_2 temperature perturbation amplitude to that of the corresponding OH temperature perturbation. We denote this wave parameter as the amplitude growth factor "G." Figure 7 plots an excellent example of terdiurnal wave growth with altitude recorded on 9–10 July (UT day 191). At the OH altitude (bottom plot), the wave amplitude was 5.1 ± 0.5 K (slightly below the mean for the 10-night ensemble) whereas the data in the upper plot indicates that the wave grew in amplitude to 9.6 ± 0.5 K by the time it reached the O_2 layer. The growth factor on this occasion was found to be 1.9 ± 0.2 which was the largest observed during this 10-day period. Significant wave growth was also observed on two other occasions (UT day 187 and 189) with magnitudes 1.6 and 1.8. Theoretically, a growth factor of ~1.7 would be expected for an ideal atmosphere (i.e., with no dissipation) due to the decrease in atmospheric density over the nominal ~7 km of mean separation of the two emission layers [*Noxon*, 1978; *Reisin and Scheer*, 1996]. For comparison, the wave analysis for the previous night (Figure 3) yielded a G factor of unity (1.0 ± 0.1) implying no measurable growth on this occasion. A similar situation arose on 5 other nights during this period (see Table 1). On one night (day 196), exceptionally strong wave dissipation was observed resulting in a 40% reduction in amplitude of the wave (from 10.2 K down to 6.3 K) over the nominal OH and O_2 height separation (see Figure 8). These examples illustrate the highly dynamic nature of the 8-hour wave during this relatively short interval in July 2002, possibly imposed by strong variability in the background atmosphere.

3.3. Eight-Hour Wind and Temperature Relation

[19] Coincident radar measurements at Maui permit a novel investigation of long-period wave signatures in mesospheric temperatures and winds. Figure 9 plots the observed winds over a 24-hour period for 87 and 94 km (mean centroid altitude of the OH and O_2 emission layers, respectively) for the 10 nights of data in July 2002 when strong 8-hour wave signatures in temperature were determined. Figures 9a and 9b show the individual zonal wind components, while Figures 9c and 9d show the corresponding meridional components. The bold curves in

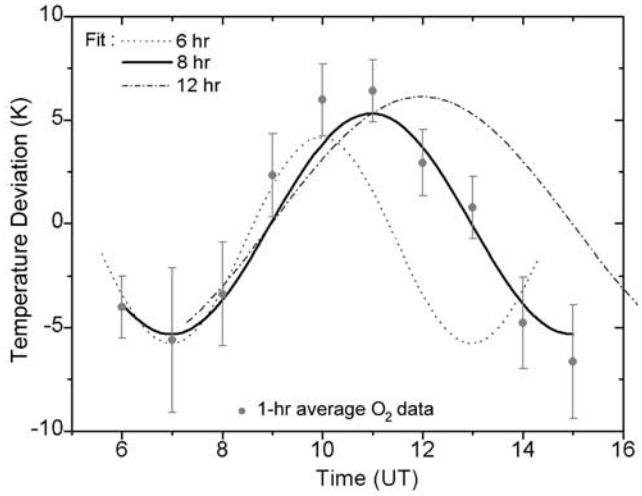

Figure 6. Average nocturnal mean O_2 temperature deviations with least squares wave fit for the wave periodicities of 6, 8, and 12 hours, illustrating their expected form for the comparison with the 10-day data ensemble.

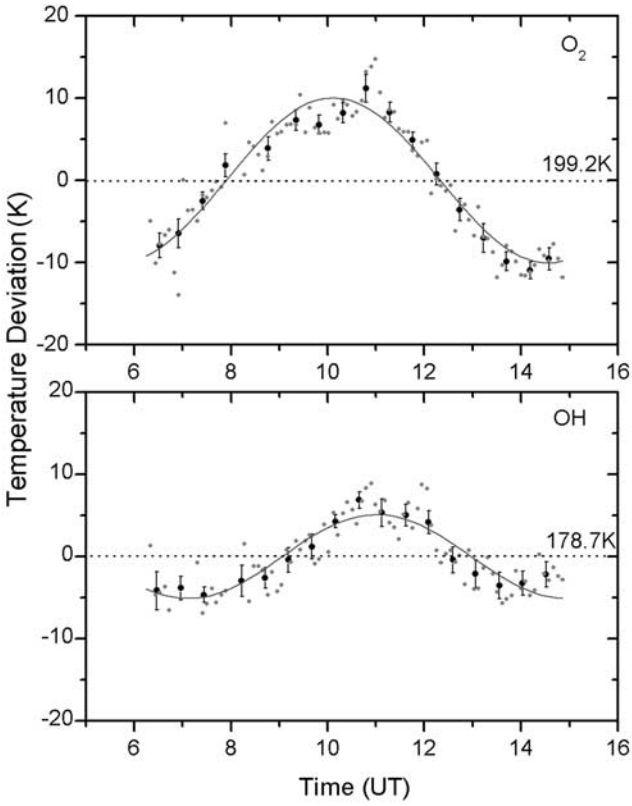

Figure 7. Example temperature data showing wave amplitude growth with altitude. The data were obtained on 9–10 July 2002 (UT day 191). The light circles show the raw data while the solid circles depict the 0.5-hour averaged data with associated standard deviations. The curves depict a best fit sinusoidal analysis yielding an ~8-hour oscillation of amplitude 5.1 ± 0.5 K in the OH data and 9.6 ± 0.5 K, yielding a growth factor of ~1.9.

each case indicate the form of the nightly mean zonal and meridional variations during this period. As expected, both the zonal and meridional wind components at 94 km exhibit larger night-to-night variability than the winds at 87 km, due primarily to the enhanced effects of gravity waves and tides. This said the meridional winds exhibit similar amplitudes (about ±40 m/s) at each emission altitude but dissimilar phase relationships. The zonal winds also exhibit similar amplitudes (~±30 m/s) but a near in-phase relation. Note that the horizontal bars in each plot indicate the nocturnal period when coincident MTM temperature measurements were made.

[20] In order to compare the wind and temperature variability at temporal scales ~8 hours, the wind data were first binned into 48-hour intervals and fitted to a model consisting of a mean, 48-, 24-, and 12-hour components. The fitted model was then subtracted from the data, leaving the residuals which contained any 8-hour (or shorter period components) present at that time. To investigate the nature of the residuals, an 8-hour component was then fitted to the residuals for each 2-day interval. The fit was weighted using the estimated standard errors for the hourly winds. This analysis revealed the intermittent nature of the 8-hour winds; however, coherent 8-hour winds of significant amplitudes (zonal and meridional) were observed during the 4 day period of 7–10 July (inclusive) permitting a direct comparison with the temperature oscillations.

[21] Figure 10 (solid line) plots the meridional wind residuals for this time interval now averaged into a 24-hour period. The corresponding temperature data averaged over the same period is indicated by the dashed lines. The top panel shows the comparison for the O_2 "wind-temperature" data while the bottom panel illustrates the results for the OH comparison. In both cases the wind and temperature perturbation amplitudes were significant at 10–15 m/s and 10–20 K peak to peak respectively, and show qualitative agreement in their temporal variability. A cross-correlation analysis was performed to help quantify the apparent relationship between the quasi-8-hour wind and temperature perturbations. This analysis showed the correlation to maximize when positive shifts were introduced in the two temperature data sets by ~2 hours (correlation 0.77 for O_2 and 0.65 for OH layer). Figure 11 shows the result of a similar analysis applied to zonal wind residuals for this period. In this case, the zonal wind component appears to be almost in anticorrelation with the quasi-8-hour temperature oscillation (correlation −0.91 for O_2 and −0.76 for OH layer when temperatures were shifted by ~1 hour). However, when temperatures were shifted by ~4 hours,

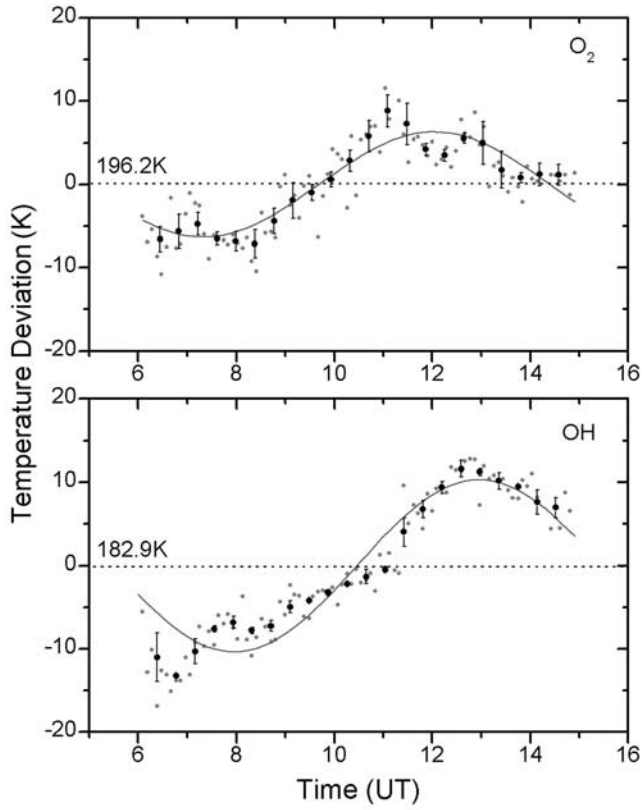

Figure 8. Example temperature data showing strong wave dissipation observed on 14–15 July 2002 (UT day 196). For comparison, the format is identical to Figure 6. On this night the terdiunal wave amplitudes were 10.2 ± 0.4 K (OH) and 6.3 ± 0.4 K (O_2), implying a G factor of 0.6.

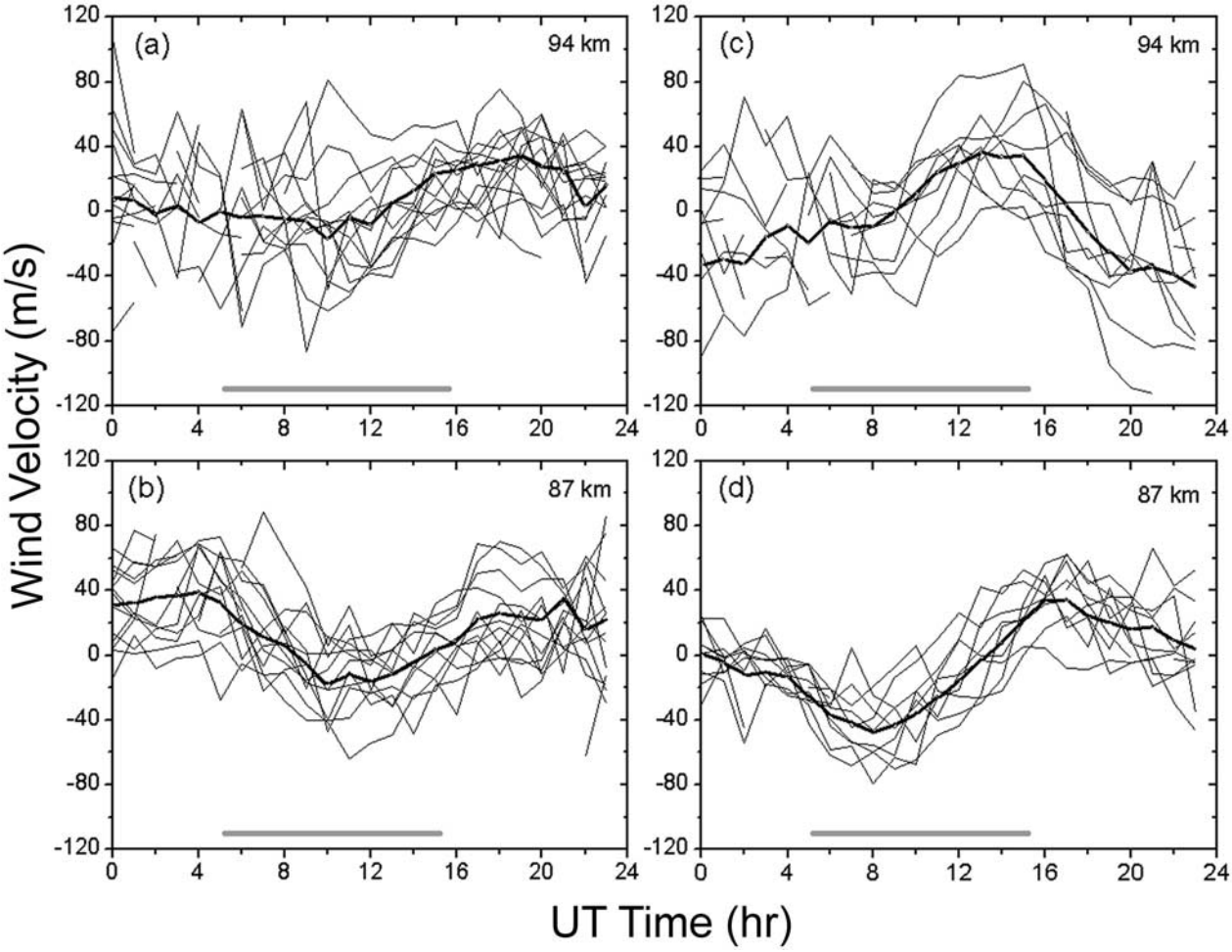

Figure 9. Ensemble of meteor radar wind data for the 10 days of coincident MTM data. (a and b) Zonal winds at 94 km (O_2) and 87 km (OH). (c and d) Respective meridional winds. In each plot the bold line depicts the mean diurnal variations during this period. The horizontal bar in each graph indicates the nocturnal duration of the coincident optical data.

the correlation with zonal wind residuals reached their maximum (0.89 for O_2 and 0.82 for OH layer).

4. Discussion

[22] Terdiurnal (8-hour) tidal oscillations in upper atmospheric winds are a well established, yet intermittent feature of the MLT region [*Avery et al.*, 1989; *Manson et al.*, 1989; *Vincent et al.*, 1989; *Franke and Thorsen*, 1993; *Thayaparan*, 1997]. Measurements from the UARS satellite have shown that the annual average of the terdiurnal tide is ~5 m/s (meridional) and 15 m/s (zonal) over the latitude range±60° at 95 km altitude [*Smith*, 2000]. The maximum amplitudes occur at midlatitudes, during fall and winter months, while amplitudes at low latitudes are usually less than 5–10 m/s. Such amplitudes are low compared with the typical semidiurnal (15–25 m/s) and diurnal (20–40 m/s) meridional and zonal components. These conditions agree well with the prevailing tidal perturbations observed over Maui during the summer 2002 (see Figure 2).

[23] In comparison, measurements of terdiurnal signatures on the mesospheric temperature are sparse and have focused on the high- (and more recently middle-) latitude mesosphere where the longer winter nights afford the best observing conditions for identifying their signatures [*Sivjee and Hamwey*, 1987; *Sivjee et al.*, 1994; *Wines et al.*, 1995; *Oznovich et al.*, 1995; *Taylor et al.*, 1999; *Pendleton et al.*, 2000]. Together, these observations (albeit limited) have revealed persuasive evidence of persistent quasi-8-hour nocturnal oscillations with mean amplitudes ~3–4 K (averaged over a several day period) and occasional nocturnal amplitudes as large as ~15 K). The detection of a well-defined terdiurnal-like wave signature in the mesospheric temperature field over Hawaii, reported here, is a novel result helping to further quantify its characteristics and demonstrating the occasional apparent dominance of this tidal harmonic at low latitudes.

4.1. Terdiurnal Temperature Oscillations at Low Latitudes

[24] This study has focused on the summer period when the GSWM model results suggested the migrating diurnal and semidiurnal tidal components of the temperature field would be at a minimum for this latitude (~20°N) [*Hagan et al.*, 1995]. Temperature amplitudes for the GSWM-02 model show a summertime minimum: semidi-

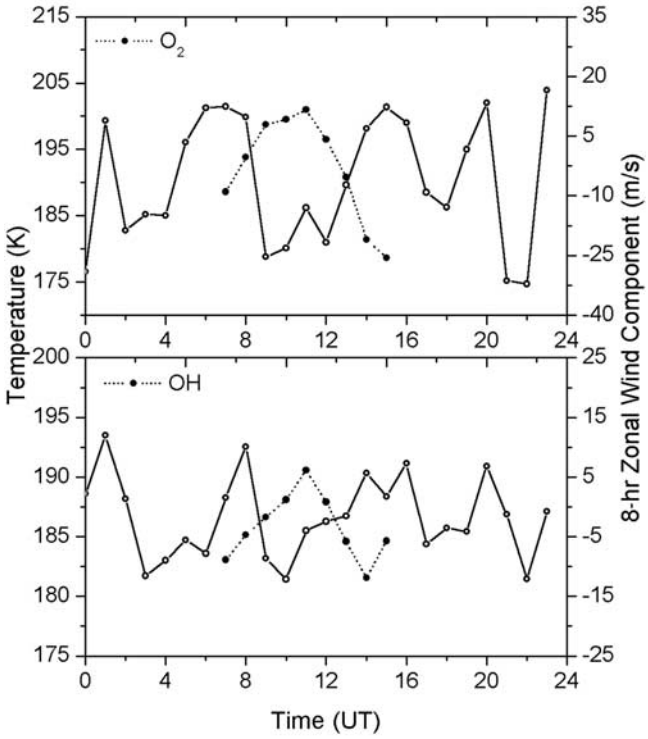

Figure 10. Time varying residual 8-hour meridional winds averaged for 7–10 July 2002 period (solid lines) plotted together with the temperature data (filled circles). (top) The wind and temperature relation for O_2 layer. (bottom) The OH layer temperature and wind variability.

urnal (~0.5 K) and diurnal (~1–2 K) amplitudes while maxima occur during the spring and fall (~3.5 and ~8 K) for the semidiurnal and diurnal components respectively (Note the GSWM-02 model does not include a terdiurnal forcing component). Thus summertime measurements are expected to be most suitable for detecting the weaker terdiurnal temperature signatures at low latitudes. However, there could also be a significant contribution to the diurnal and semidiurnal tidal wind field caused by nonmigrating components, but these are as yet not well defined [e.g., *Hecht et al.*, 1998; *Talaat and Lieberman*, 1999].

[25] The detection of relatively large amplitude waves in the OH and O_2 temperature data (typically ~10 K for individual nights and average ~5–6 K) is significant and suggests potentially strong terdiurnal-type forcing at low latitudes during this 10-day period in July. In comparison, studies of the terdiurnal temperature signatures at midlatitudes (which have been conducted primarily from Bear Lake Observatory, Utah, 41.9°N) over a similar duration (10-day period) indicated a mean nocturnal temperature amplitude of ~3–4 K during the fall and early winter months when UARS satellite data also indicated strong terdiurnal activity in the mesospheric wind field [*Wines et al.*, 1995; *Pendleton et al.*, 2000].

[26] The observed range in our 8-hour temperature amplitudes (5.1 to 16.8 K) is large but consistent with those reported by *Pendleton et al.* [2000] using OH measurements alone and emphasizes the occasional prominence of this wave component. For example, published measurements of the semidiurnal tide (which is expected to be much stronger), from Hawaii (20.8°N) during the ALOHA-93 campaign [*Hecht et al.*, 1995] show individual OH wave amplitudes ranging from 1.5 to 6.9 K with a mean of ~3.5 K in good agreement with the GSWM-02 model. Furthermore, OH measurements of the semidiurnal tidal component observed at a midlatitude site from Argentina (32°S) show a significantly larger mean amplitude ~11 K (as recorded during a several month period) yet the range of individual semidiurnal measurements (7–15 K) is similar to that reported here (5.1 to 16.8 K) for the terdiurnal temperature component.

[27] Additional evidence in support of a terdiurnal tidal interpretation for these data is obtained from phase information determined from wave fitting to the temperature measurements from the two emission layers. Figure 12a plots the phase difference (O_2 −OH) as a function of day number for each of the 10 nights of data. Individual phase separations range from 0.5 to 2.0 hours (see Table 1) with a clear dominance for a mean of ~1.0 hour. On the last night of the observations, the phase shift jumped to ~2 hours for the same "goodness" of wave fit. Importantly, the O_2 wave perturbation always led the OH temperature variation providing strong evidence of downward phase progression associated with this 8-hour wave, consistent with its generation in the lower atmosphere directly by solar heating or by dynamical wave-wave interactions between other tidal components [e.g., *Smith*, 2000]. Assuming a mean separation in altitude of 7 km for the OH and the O_2 emission layers we can estimate the downward phase velocity associated with each of these long-period wave events. The results are listed in Table 1 and indicate phase speeds of 0.9–3.8 m/s with a mean of 2.3 m/s. Applying these results to an ~8-hour wave motion yields vertical wavelengths in

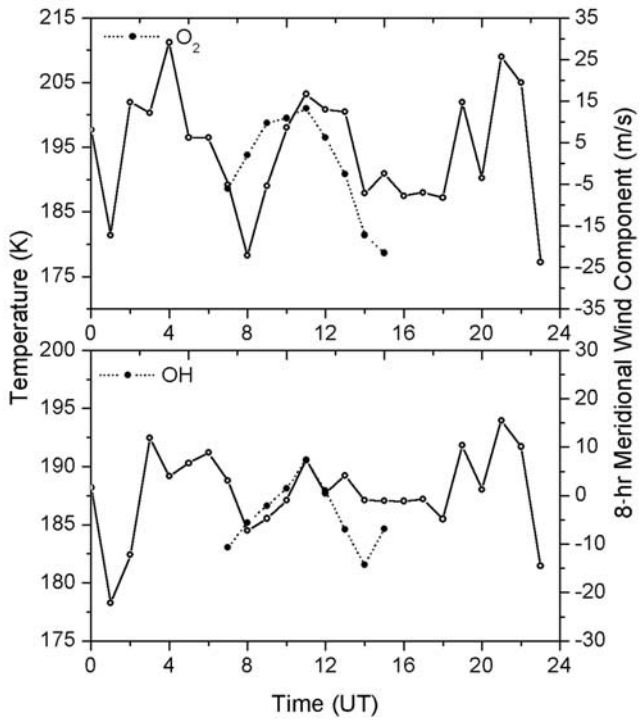

Figure 11. Same as Figure 10 but for residual 8-hour zonal winds.

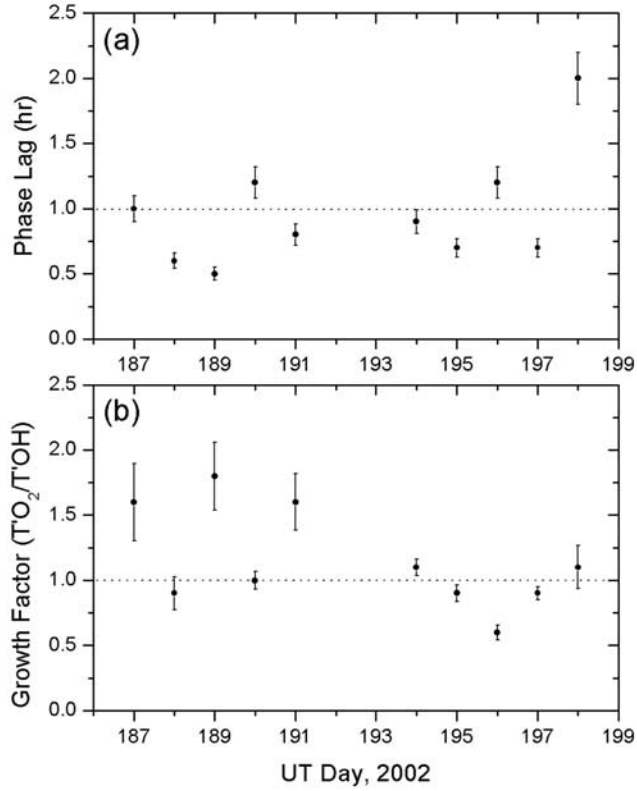

Figure 12. Summary plot showing (a) the variability in the phase difference and (b) the derived growth factors "G" for the 10 nights of data. Large variations in the G factor are evident (range 0.6–1.9), while the phase shift exhibited little variability (mean ~1 hour) throughout this period.

the range 26–110 km with a mean of 63 km. Recently Smith et al. (2001) have computed vertical wavelengths for various global Hough modes (1–7) for terdiurnal tidal winds. Several of these modes (3–7) fall within the range 47–116 km which agrees well with our vertical wavelength estimates from mesospheric temperature measurements. In particular, the averaged temperature data indicates a vertical wavelength of 62.7 km which compares very favorably with the #5 wind Hough mode (63 km). Unfortunately, there are currently no model predictions for terdiurnal temperatures as a function of latitude to directly compare our measurements with.

4.2. Terdiurnal Wave Amplitude and Growth

[28] As well as measurements of the phase relation, we can also use the amplitude growth factor "G" to further investigate the wave dynamics in this part of the MLT region. Figure 12b plots G versus day number for the July data set. As discussed earlier, under ideal conditions with no wave dissipation, the amplitude of the 8-hour tide would be expected to grow by a factor of ~1.7, as detected in the OH and O_2 emission layers. The figure shows that on ~60% of the nights the 8-hour wave exhibited a G factor close to unity implying no measurable wave growth with altitude. In comparison, only three nights (30%) exhibited growth factors in the range of ~1.6–1.9 expected under conditions of no significant wave dissipation. These three events occurred earlier in our observing period but were not consecutive. We are unaware of any prior measurements of wave growth (or dissipation) for 8-hour oscillations at mesospheric heights. This said, we note here that midlatitude measurements of long period (~10–14 hours) waves observed in the OH and O_2 emission by *Reisin and Scheer* [1996] show a similar range of growth factors of 0.5–1.9. However, in their case the wave perturbations were attributed primarily to the semidiurnal tide. The calculation of the wave amplitude growth and implications on the wave dissipation depend critically on the assumption of the airglow layer height separation. For example, the observed G factors in the range 1.6–1.9 correspond to a nominal altitude separation of ~6.5–9 km for dissipationless atmosphere.

[29] During this observation period, there were no simultaneous measurements of the OH and O_2 layer profiles; however, height changes of this magnitude are quite possible, especially under conditions of strong tidal forcing [e.g., *Melo et al.*, 2001; *Zhao et al.*, 2005]. However, the majority of our measurements indicate a G factor of close to unity which suggests either significant wave damping or similar altitudes for the two layers. If the later were the case there should be no phase difference between the 8-hour waves simultaneously observed in the OH and O_2 temperature data. Figure 12a shows a clear phase shift for these six nights ranging from 0.6 to 2.0 hours with a mean of 1.0 hours, implying sizable separation of the layer centroids, and consequently wave dissipation. Regardless of the layer separation uncertainty, the observation of a G factor of ~0.6 on day 196 suggests strong wave dissipation. Taken together, these measurements show clear evidence for wave dissipation, of variable magnitude during this relatively short 10-day period in July.

4.3. Terdiurnal Temperature and Wind Relation

[30] The observation of a strong correlation between the tidally induced temperature and wind variability is not surprising as the temperature and wind perturbations are driven by the same wave forcing (in this case an ~8-hour period wave). Such studies are rare, probably because of the apparent lack of coincident temperature and 24-hour wind measurements over extended periods of time. However, *Hocking and Hocking* [2002] have investigated the wind-temperature relationship for diurnal and semidiurnal tides using Meteor Wind Radar and inferred temperature studies. The Maui MALT program is designed to investigate mesospheric dynamics at low latitudes using complementary optical and radar observing techniques and provides the opportunity for further such detailed coordinated measurements.

[31] Our observations (Figures 10 and 11) show coherent structure and a clear phase shift between the terdiurnal wind and mesospheric temperatures as measured at two altitudes (with the temperature variation apparently lagging the wind components). In particular, the meridional wind component shows a smaller phase shift of ~2 hours than that of the zonal wind component (~4 hours). In comparison, the recent study by *Hocking and Hocking* [2002] shows the meridional wind component to be almost in phase for the upward propagating semidiurnal tide for vertical wavelength smaller than 80 km while substantial phase shifts

between temperature and zonal wind component are expected resulting in a quadratic relationship (due to the forcing of the meridional circulation by zonal energy dissipation). For much larger vertical wavelengths (when the tidal modes approach evanescence), the temperature oscillations were shown to be almost in-phase with zonal winds while, for moderately long vertical wavelengths, it is expected that the observed zonal and meridional phase relationship will lie between these limits. Their investigation utilized midlatitude measurements; however, the associated theoretical study extended from 20 to 50°N which includes Hawaii (20.8°N). Although the Hocking and Hocking study focused on the semidiurnal and diurnal tidal component, it is not unreasonable to assume that a similar relationship may exist for the terdiurnal component discussed herein. This has yet to be established. However, our findings on the phase relation for quasi-8-hour temperature and wind components (2 hours for meridional and 4 hours for zonal component) for moderately long inferred vertical wavelengths of 52–113 km during the 7–10 July period agree well with the ideas put forth by *Hocking and Hocking* [2002].

5. Summary

[32] This study provides new measurements of quasi-8-hour oscillation in mesospheric temperature at low latitudes. This oscillation appears to be indicative of the terdiurnal tidal component for the following reasons:

[33] 1. Average of highly coherent oscillations observed over a 10-day period exhibits a well-defined terdiurnal signature with similar mean amplitudes of ~5.5 K in both OH and O_2 emissions.

[34] 2. Consistent and well-defined phase shift (average ~1 hour) implying downward phase progression supporting a lower atmospheric origin for the oscillation.

[35] 3. Deduced vertical wavelength (average ~63 km) compares very favorably with that predicted by the Rose model for the terdiurnal wind [*Smith and Ortland*, 2001].

[36] 4. Novel investigations of the induced 8-hour temperature and mesospheric wind variability comparison suggest a significant correlation with a discernable phase shift.

[37] This oscillation was a dominant feature of the nocturnal MLT temperature field during a 10-day period in July 2002. Observations of terdiurnal oscillations in mesospheric temperature are rare and these measurements provide the first experimental data at low latitudes. Furthermore, detailed measurements of the growth of this wave component show amplification factors ranging from 0.6 to 1.9 suggesting variable degrees of wave dissipation over the nominal altitude range 87–94 km. This in turn implies that the low-latitude mesospheric region can be highly dynamic (at least during July). However, our MTM data suggest that this wave activity may extend to longer intervals during the summer. Finally, we report new observations demonstrating an apparent phase relationship between the OH and O_2 temperatures and the zonal and meridional wind residuals for the 8-hour tide. Further analysis of our joint wind and temperature data for other summer months and seasons is planned.

[38] **Acknowledgments.** We are most grateful to P. Kervin, Director of the Maui AEOS Facility, which continues to support the Maui MALT measurements program. We kindly acknowledge the Boeing support staff, and in particular, we wish to thank R. Taft and S. Ah You for their unstinting help with the operation of our instrumentation. We thank M. Hagan (NCAR) for the use of the GSWM model and for her important advice on our tidal measurements, and we thank W. R. Pendleton Jr., Y. Zhao, and P.-D. Pautet (USU) for their very helpful discussions. We also wish to extend our thanks to C. S. Gardner and G. R. Swenson for their leadership in this program. This research was conducted as part of an ongoing joint program between the Air Force Office of Scientific Research (AFOSR) and the National Science Foundation (NSF). Financial support for the USU- MTM for Maui MALT program was provided by NSF grant ATM-0003218 and for Meteor radar observations and data analysis were supported by NSF grants ATM-00-3182 and ATM-00-3198. As part of this research, A. Taori was supported as a CEDAR postdoctoral fellow under NSF grant ATM-0134150.

References

Akmaev, R. A. (2001), Seasonal variations of the terdiurnal tide in the mesosphere and lower thermosphere: A model study, *Geophys. Res. Lett.*, *28*, 3817–3820.

Avery, S. K., R. A. Vincent, A. Phillips, A. H. Manson, and G. J. Fraser (1989), High latitude tidal behavior in the mesosphere and lower thermosphere, *J. Atmos. Terr. Phys.*, *51*, 508–595.

Burrage, M. D., M. E. Hagan, W. R. Skinner, D. L. Wu, and P. B. Hays (1995), Long term variability in the solar diurnal tide observed by HRDI and simulated by GSWM, *Geophys. Res. Lett.*, *22*, 2641–2644.

Chapman, S., and R. S. Lindzen (1970), *Atmospheric Tides*, Springer, New York.

Crary, D. J., and J. M. Forbes (1983), On the extraction of tidal information from measurements covering a fraction of a day, *Geophys. Res. Lett.*, *10*, 580–582.

Dao, P. D., R. Farley, X. Tao, and C. S. Gardner (1995), Lidar observations of the temperature profile between 25 and 103 km: Evidence of strong tidal perturbations, *Geophys. Res. Lett.*, *22*, 2825–2828.

Franke, S. J., and D. Thorsen (1993), Mean winds and tides in the upper middle atmosphere at Urbana (40°N, 88°W) during 1991–1992, *J. Geophys. Res.*, *98*, 18,607–18,615.

Fukuyama, K. (1976), Airglow variations and dynamics in the lower thermosphere and upper mesosphere-1, Diurnal variation and its seasonal dependency, *J. Atmos. Terr. Phys.*, *38*, 1279–1287.

Glass, M., and J. L. Fellous (1975), The eight-hourly (ter-diurnal) component of atmospheric tides, *Space Res.*, *15*, 191–197.

Goldman, A., W. G. Schoenfeld, D. Goorvitch, C. Chackerian Jr., H. Dothe, F. Mélen, M. C. Abrams, and J. E. A. Selby (1998), Updated line parameters for the OH $X^2\Pi$-$X^2\Pi(v'', v')$ transitions, *J. Quant. Spectrosc. Radiat. Transfer*, *59*, 453–469.

Hagan, M. E., J. M. Forbes, and F. Vial (1995), On modeling migrating solar tides, *Geophys. Res. Lett.*, *22*, 893–896.

Hays, P. B., D. L. Wu, M. D. Burrage, D. A. Grell, H. J. Grassl, R. S. Lieberman, A. R. Marshall, Y. T. Morton, D. A. Ortland, and W. R. Skinner (1994), Observations of diurnal tide from space, *J. Atmos. Sci.*, *51*, 3077–3093.

Hecht, J. H., S. K. Ramsay Howat, R. L. Walterscheid, and J. R. Isler (1995), Observations of variations in airglow emissions during ALOHA-93, *Geophys. Res. Lett.*, *22*, 2817–2820.

Hecht, J. H., et al. (1998), A comparison of atmospheric tides inferred from observations at the mesopause during ALOHA-93 with the model predictions of the TIME-GCM, *J. Geophys. Res.*, *103*, 6307–6321.

Hocking, W. K., and A. Hocking (2002), Temperature tides determined with meteor radar, *Ann. Geophys.*, *20*, 1447–1467.

Hocking, W. K., and T. Thayaparan (1997), Simultaneous and collocated observation of winds and tides by MF and meteor radar over London, Canada, *Radio Sci.*, *32*(2), 833–865.

Manson, A. H., C. E. Meek, H. Teielbaum, F. Vial, R. Schminder, D. Kurschner, J. J. Smith, and G. J. Fraser (1989), Climatologies of semi-diurnal and diurnal tides in the middle atmosphere (70–110 km) at middle latitudes (40–55°), *J. Atmos. Terr. Phys.*, *51*, 579–593.

Melo, S. M. L., R. P. Lowe, W. R. Pendleton Jr., M. J. Taylor, B. Williams, and C. Y. She (2001), Effects of a large mesospheric temperature enhancement on the hydroxyl rotational temperature as observed from the ground, *J. Geophys. Res.*, *106*(A12), 30,381–30,388.

Meriwether, J. W. (1984), Ground based measurements of mesospheric temperatures by optical means, in *Middle Atmosphere Program Handbook for MAP*, vol. 13, edited by R. Vincent, pp. 1–18, NASA, Greenbelt, Md.

Namboothiri, S. P., P. Kishore, Y. Muruyama, and K. Igarashi (2004), MF radar observations of terdiurnal tide in the mesosphere and lower thermosphere at Wakkanai, Japan, *J. Atmos. Sol. Terr. Phys.*, *66*, 241–250.

Noxon, J. F. (1978), Effects of internal gravity waves upon night airglow temperatures, *Geophys. Res. Lett.*, *5*(1), 25–27.

Oznovich, I., D. J. McEwen, and G. G. Sivjee (1995), Temperature and airglow brightness oscillations in the polar mesosphere and lower thermosphere, *Planet. Space Sci.*, *43*, 1121–1130.

Pendleton, W. R., M. J. Taylor, and L. C. Gardner (2000), Terdiurnal oscillations in OH Meinel rotational temperatures for fall conditions at northern mid-latitude sites, *Geophys. Res. Lett.*, *27*(12), 1799–1802.

Petitdidier, M., and H. Teitelbaum (1977), Lower thermosphere emissions and tides, *Planet. Space Sci.*, *25*, 711–721.

Reisin, E. R., and J. Scheer (1996), Characteristics of atmospheric waves in the tidal period range derived from zenith observations of O_2(0,1) Atmospheric and OH (6,2) airglow at lower midlatitudes, *J. Geophys. Res.*, *101*, 21,223–21,232.

Revah, I. (1969), Etude des vents de petite, échelle observes au moyen des trainees meteoriques, *Ann. Geophys.*, *25*(1), 1–45.

She, C. Y., et al. (2003), The first 80-hour continuous lidar campaign for simultaneous observation of mesopause region temperature and wind, *Geophys. Res. Lett.*, *30*(6), 1319, doi:10.1029/2002GL016412.

Shepherd, G. G., C. McLandress, and B. H. Solheim (1995), Tidal influence on O(^{1}S) airglow altitudes and emission rates at the geographic equator observed by WINDII, *Geophys. Res. Lett.*, *22*, 275–278.

Sivjee, G. G., and R. M. Hamwey (1987), Temperature and chemistry of the polar mesopause OH, *J. Geophys. Res.*, *92*, 4663–4672.

Sivjee, G. G., R. L. Walterscheid, and D. J. McEwen (1994), Planetary wave disturbances in the Arctic winter mesopause over Eureka (80°N), *Planet. Space Sci.*, *42*, 447–453.

Smith, A. K. (2000), Structure of the terdiurnal tide at 95 km, *Geophys. Res. Lett.*, *27*(2), 177–180.

Smith, A. K., and D. A. Ortland (2001), Modeling and analysis of the structure and generation of the terdiurnal tide, *J. Atmos. Sci.*, *58*, 3116–3134.

States, R. J., and C. S. Gardner (2000), Thermal structure of the mesopause region (80–105 km) at 40°N latitude. Part II: Diurnal variations, *J. Atmos. Sci.*, *57*, 78–92.

Takahashi, H., Y. Sahai, and P. P. Batista (1984), Tidal and solar cycle effects on the OI5577A, NaD and OH (8,3) airglow emissions observed at 23S, *Planet. Space Sci.*, *32*, 897–902.

Talaat, E. R., and R. S. Lieberman (1999), Nonmigrating diurnal tides in mesospheric and lower-thermospheric winds and temperatures, *J. Atmos. Sci.*, *56*, 4073–4087.

Taylor, M. J., W. R. Pendleton Jr., C. S. Gardner, and R. J. States (1999), Comparison of terdiurnal tidal oscillations in mesospheric OH rotational temperatures and Na lidar temperature measurements at mid-latitudes for fall/spring conditions, *Earth Planets Space*, *51*, 877–885.

Taylor, M. J., L. C. Gardner, and W. R. Pendleton Jr. (2001), Long period wave signatures in mesospheric OH Meinel (6,2) band intensity and rotational temperature at mid latitudes, *Adv. Space Res.*, *27*(6–7), 1171–1179.

Teitelbaum, H., F. Vial, A. H. Manson, R. Giraldez, and M. Massebeuf (1989), Nonlinear interaction between the diurnal and semidiurnal tides: Terdiurnal and diurnal secondary waves, *J. Atmos. Terr. Phys.*, *51*, 627–634.

Thayaparan, T. (1997), The terdiurnal tide in the mesosphere and lower thermosphere over London, Canada (43°N, 81°W), *J. Geophys. Res.*, *102*, 21,695–21,708.

Vincent, R. A., T. Tsuda, and S. Kato (1989), Asymmetires in mesospheric tidal structure, *J. Atmos. Terr. Phys.*, *51*, 609–616.

Walterscheid, R. L., G. G. Sivjee, G. Schubert, and R. M. Hamwey (1986), Large amplitude semi-diurnal variations in the polar mesopause: Evidence of a pseudotide, *Nature*, *324*, 347–349.

Wines, R. H., S. P. Zhang, R. Peterson, and G. G. Shepherd (1995), Tides in emission rate and temperature from the O_2 nightglow over Bear Lake Observatory, *Geophys. Res. Lett.*, *22*, 2637–2640.

Younger, P. T., D. Pancheva, H. R. Middleton, and N. J. Mitchell (2002), The 8-hour tide in the Arctic mesosphere and lower thermosphere, *J. Geophys. Res.*, *107*(A12), 1420, doi:10.1029/2001JA005086.

Zhao, Y., M. J. Taylor, and X. Chu (2005), Comparison of simultaneous Na lidar and mesospheric nightglow temperature measurements and the effects of tides on the emission layer heights, *J. Geophys. Res.*, *110*, D09S07, doi:10.1029/2004JD005115.

S. Franke, Department of Electrical and Computer Engineering, University of Illinois, Urbana, IL 61802, USA. (s-franke@uiuc.edu)

A. Taori and M. J. Taylor, Center for Atmospheric and Space Sciences, Utah State University, Logan, UT 84341, USA. (alok@cc.usu.edu; mtaylor@cc.usu.edu)